EUROPEAN ORGANIZATION FOR NUCLEAR RESEARCH

CERN-EP/83-130
7 September 1983

HIGH-p_T PHYSICS AT THE CERN INTERSECTING STORAGE RINGS

T. Åkesson

CERN, Geneva, Switzerland

Invited talk given at the
14th International Symposium on Multiparticle Dynamics,
Lake Tahoe, Calif., USA, 22-27 June 1983

HIGH-p_T PHYSICS AT THE CERN INTERSECTING STORAGE RINGS

Torsten Åkesson

CERN
CH-1211 Geneva 23
SWITZERLAND

ABSTRACT

Recent experimental results in high-p_T physics at the ISR are reviewed. Emphasis is laid on calorimeter-triggered events and the dominance of jets at high E_T. Jet fragmentation in pp interactions is compared with e^+e^- annihilations, and charge compensation in jet events is discussed.

1. Introduction

In the summer of 1982 a long-expected result in high-p_T physics--the emergence of jets in high-E_T calorimeter-triggered events--was presented at the 21st Int. Conf. on High-Energy Physics, Paris. The observation was made by the UA2 experiment at the CERN $p\bar{p}$ Collider[1a] and by the Axial Field Spectrometer (AFS) at the Intersecting Storage Rings (ISR)[1b]. This was followed at the ISR by a measurement of the inclusive jet cross-section at $\sqrt{s}$ = 63 GeV [2] and $\sqrt{s}$ = 45 GeV[3], and by the energy dependence of the jet cross-section[3]. At the collider, UA2 presented the inclusive jet cross-section at $\sqrt{s}$ = 540 GeV [4] and UA1 showed evidence for jet dominance in high-E_T events[5].

Here I will present new results from the ISR. I will concentrate on the analysis of calorimeter-triggered events. The data reported come from two spectrometers: that of the CERN-Oxford-Rockefeller (COR) experiment[6] in intersection 1 (Fig. 1) and the neighbouring AFS [7] (Fig. 2) in intersection 8.

2. Transverse energy spectra and jet dominance

The COR experiment measures the transverse energy with a combination of shower counters and lead-glass blocks. Since this equipment ideally measures energy only from particles giving electromagnetic showers, mainly π^0's COR make their analysis as a function of total neutral transverse energy E_T^0. Figure 3 shows their distribution of neutral transverse energy. The data correspond to an integrated luminosity of 2.7×10^{37} cm^{-2}. The distribution is not corrected for effects from the apparatus. At the AFS the energy measurement is made with a combined electromagnetic and hadronic calorimeter and hence the total transverse energy E_T is measured. The AFS calorimeter is a sandwich of uranium, copper, and scintillator

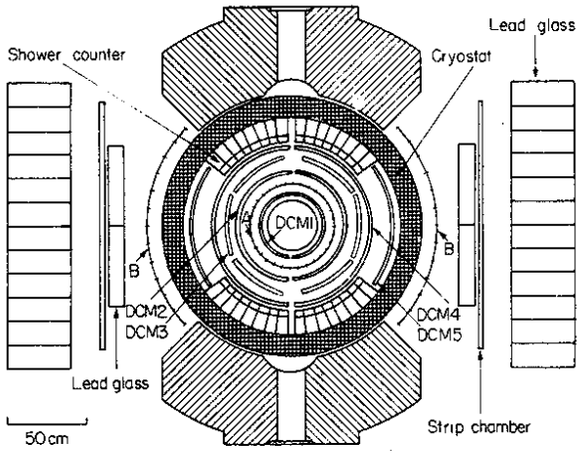

	Shower counters	Lead glass
$\Delta\Phi$	4×50^0	2×57^0
$\|y\|<$	1.1	0.6
depth	$14\chi^0$	$21\chi^0$
$\Delta E/E$	$16\%/\sqrt{E}$	$(4.3/\sqrt{E}+2)\%$

Fig. 1 The COR experimental set-up.

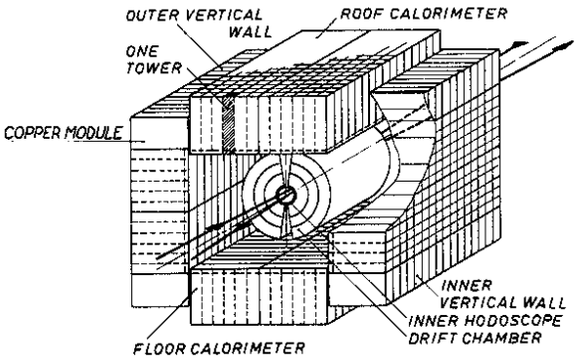

Calorimeter

$\Delta\varphi$	100%
$\|y\|<$	0.9
depth	3.6λ
$\delta E/E$(em)	$16\%/\sqrt{E}$
$\delta E/E$(had)	$37\%/\sqrt{E}$

Fig. 2 The AFS experimental set-up.

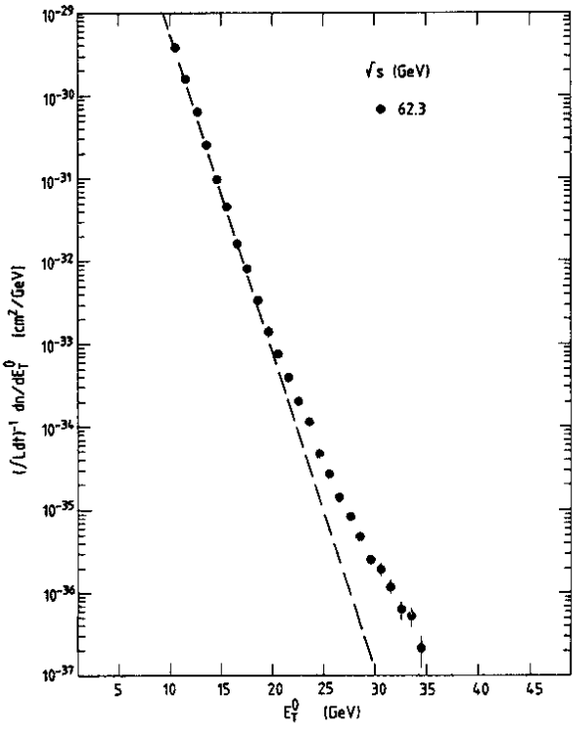

Fig. 3 Uncorrected spectrum for neutral transverse energy measured by the COR Collaboration at $\sqrt{s}$ = = 63 GeV.

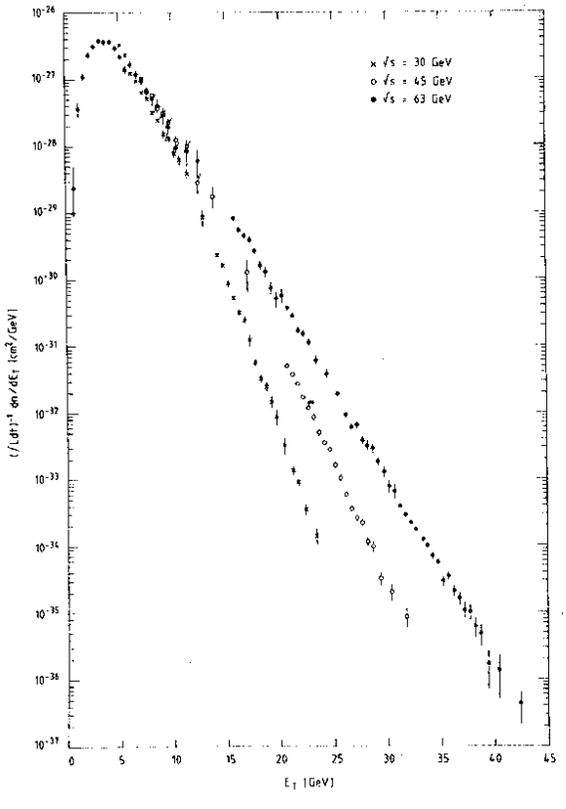

Fig. 4 Uncorrected spectrum of transverse energy measured by the AFS at $\sqrt{s}$ = 30, 45 and 63 GeV.

planes, and has a unique energy resolution of hadronic showers (see Fig. 2). Figure 4 shows the distributions of total transverse energy measured by the AFS at three different centre-of-mass energies, 30, 45, and 63 GeV, corresponding to the integrated luminosities of 9.9×10^{34}, 6.8×10^{35}, and 3×10^{36} cm^{-2}. These spectra are also uncorrected for apparatus effects. It should be noted that the 63 GeV measurement spans 10 orders of magnitude in cross-section.

We will now examine the character of the events as a function of the total transverse energy. To do this, the variable circularity C has been used by the AFS. The circularity is the two-dimensional equivalent of sphericity: C = 0 for a perfect "pencil-like" jet event and C = 1 for a spherical event. The plane in which the circularity is calculated is, of course, perpendicular to the beam direction. Figure 5 shows the mean circularity versus E_T for the three different centre-of-mass energies. It can be seen that $\langle C \rangle$ stays rather constant up to $E_T \sim 25$ GeV, above which it falls quickly. An interesting feature is how independent of $\sqrt{s}$ the points are; the variation of $\langle C \rangle$ seems, to a first order, to be a function of E_T only. This does not, of course, mean that the centre-of-mass energy is unimportant, since the cross-section for measuring high E_T is much greater at a larger $\sqrt{s}$ (Fig. 4). The circularity distributions themselves are shown in Fig. 6. At high E_T a striking peak at low circularity emerges, and in the highest E_T bin the low-circularity events dominate completely. The COR Collaboration observes the same phenomena. In bins of E_T^0 they calculate sphericity*) S using information from both the calorimeters and the charged tracks in the drift chambers. The sphericity distributions in two E_T^0 bins are shown in Fig. 7a and exhibits a complete dominance by the low-sphericity events in the high E_T^0 bin. The mean sphericity is also continuously falling from $E_T^0 \approx 14$ GeV (Fig. 7b).

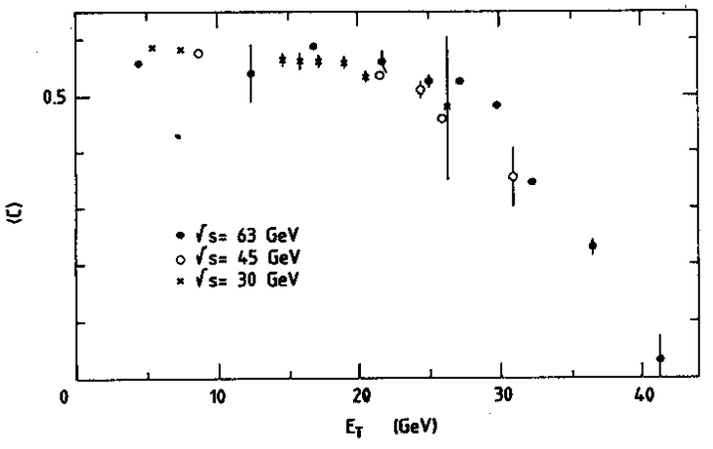

Fig. 5 Mean circularity versus E_T measured by the AFS.

*) The variable called circularity by the AFS is called sphericity by the COR group.

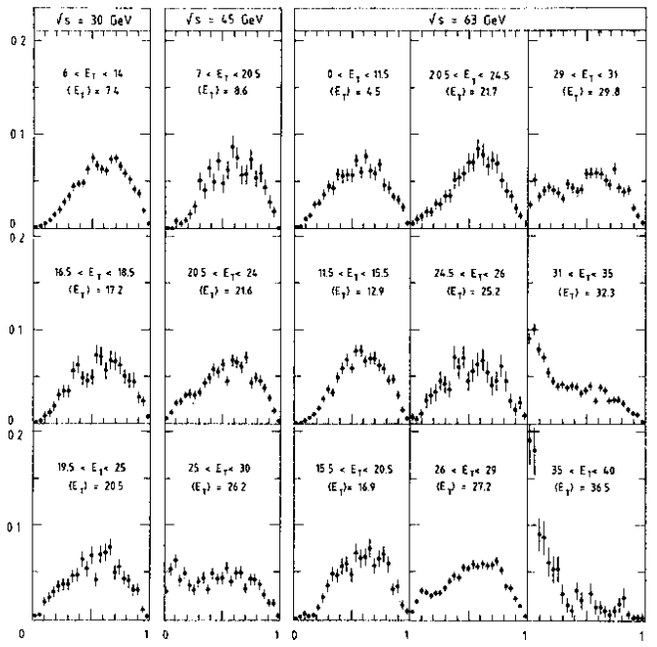

Fig. 6 Circularity distributions measured by the AFS.

In Fig. 3 it is seen that the E_T^0 spectrum deviates from an exponential in the same region as where the change in event structure occurs. A corresponding effect is not observed in Fig. 4, the AFS measurement, but it should be pointed out that both spectra are uncorrected for apparatus effects. The COR Collaboration measures with electromagnetic calorimeters only, so a correction to their E_T^0 is dominated by resolution of the shower measurement, and by dE/dx and nuclear interactions from particles not giving electromagnetic showers. All these effects cause the apparatus to overestimate E_T^0. In addition, the fraction of the total E_T carried by E_T^0 is not constant with E_T^0. The AFS Collaboration measures with an electromagnetic and hadronic calorimeter, but here the apparatus effect is dominated at high E_T by leakage of the hadronic showers. This effect causes the apparatus to underestimate E_T. To summarize: Correcting the COR spectrum (Fig. 3) would tend to decrease the deviation from an exponential, whilst the correction to the AFS spectrum would produce a deviation from an exponential. The result is that no strong conclusion can be drawn from the spectra, but it would be strange if the strong change in event shape were not accompanied by an effect in the E_T distributions.

Figure 8a shows the fraction of E_T^0 in the two largest clusters and in the largest cluster measured by the COR shower and lead-glass counters.

The clustering procedure described in Ref. 8 gives not a fixed cluster size but the increase (in cluster size) is rather modest with E_T^0. The increasing fractions show just the behaviour expected from jet events. The fraction of events with more than 60% of their E_T in two non-overlapping regions of $\Delta y = 1$, $\Delta\phi = 60^\circ$, is shown in Fig. 8b. This is a measurement of the AFS and clearly shows the jet dominance at high-E_T. Also, here the relative $\sqrt{s}$ independence is observed.

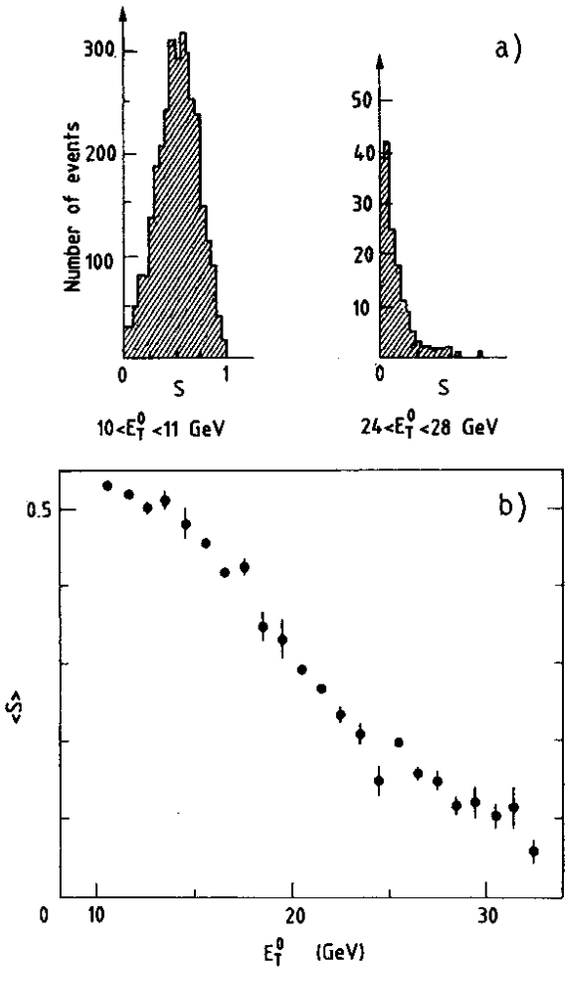

Fig. 7 a) Sphericity distributions in two regions of E_T^0. b) Mean sphericity versus E_T^0.

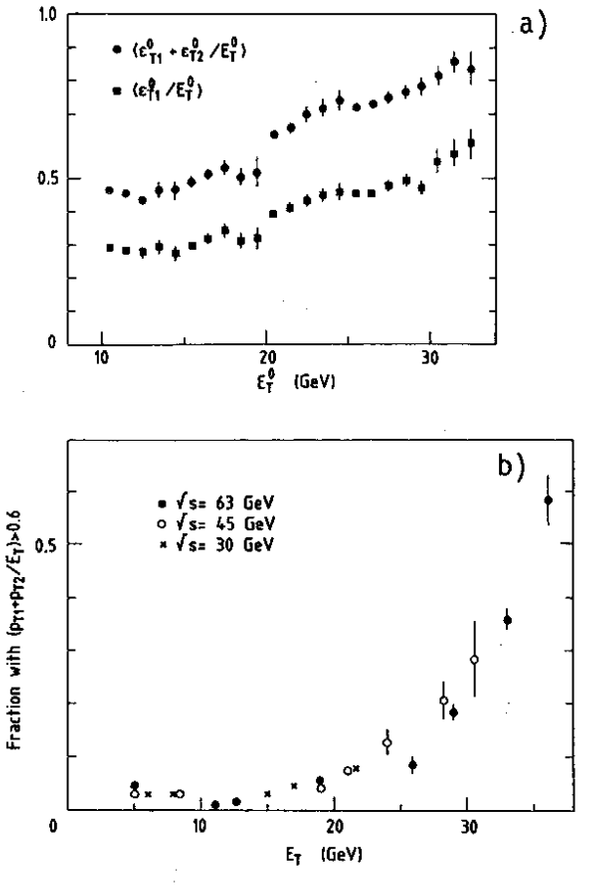

Fig. 8 a) The mean fraction of neutral transverse energy contained in the two most energetic clusters (squares) and the mean fraction of neutral transverse energy contained in the most energetic cluster (circle), versus E_T^0. b) Fraction of events with more than 60% of their E_T in two non-overlapping regions of $\Delta\phi = 60^\circ$ and $\Delta y = 1$, versus E_T.

The back-to-back nature of the two jets is demonstrated by the COR Collaboration. They find the jet direction using the following algorithm:

i) split the event into two hemispheres;
ii) calculate the vector sum of the momenta in each hemisphere, $\vec{p}_1$ and $\vec{p}_2$;
iii) split the event into two new hemispheres by taking the normal to the largest of $\vec{p}_1$ and $\vec{p}_2$;
iv) repeat (ii) and (iii) until the process has converged.

The azimuthal angle between $\vec{p}_1$ and $\vec{p}_2$ is shown in Fig. 9a and clearly demonstrates the back-to-back nature of the jets. The AFS Collaboration have used a cluster algorithm described in the next section and in Ref. 9. The azimuthal angle between the two jet axes found is plotted in Fig. 9b, and here it is also shown that the jets are opposite each other.

As a final illustration of the nature of the events at high E_T, Fig. 10 shows some events with $E_T > 35$ GeV measured by the AFS.

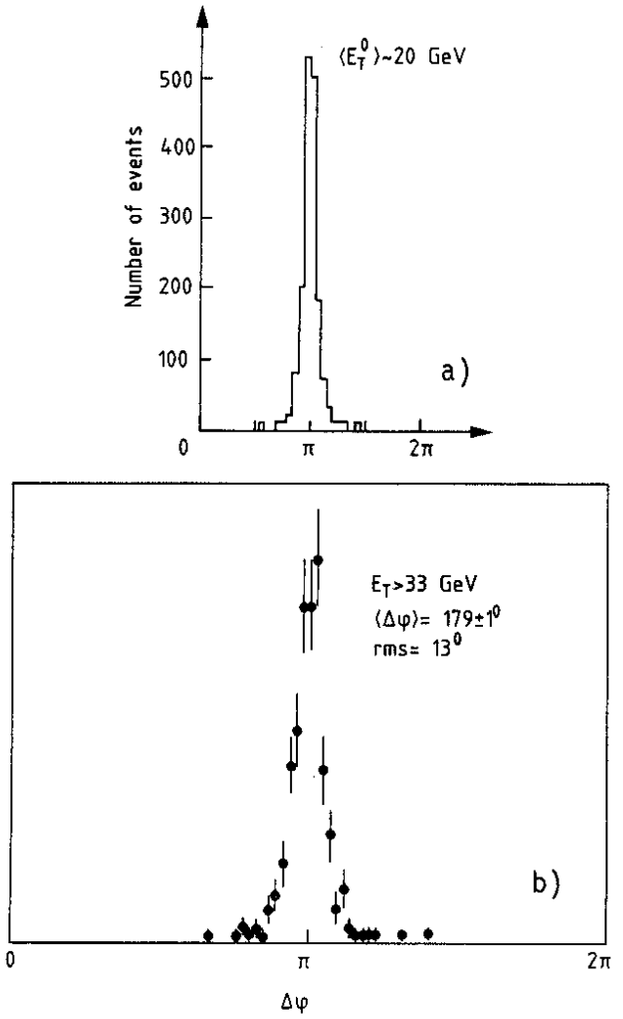

Fig. 9 The azimuthal angle between the two jet axes defined in the text. a) COR; b) AFS.

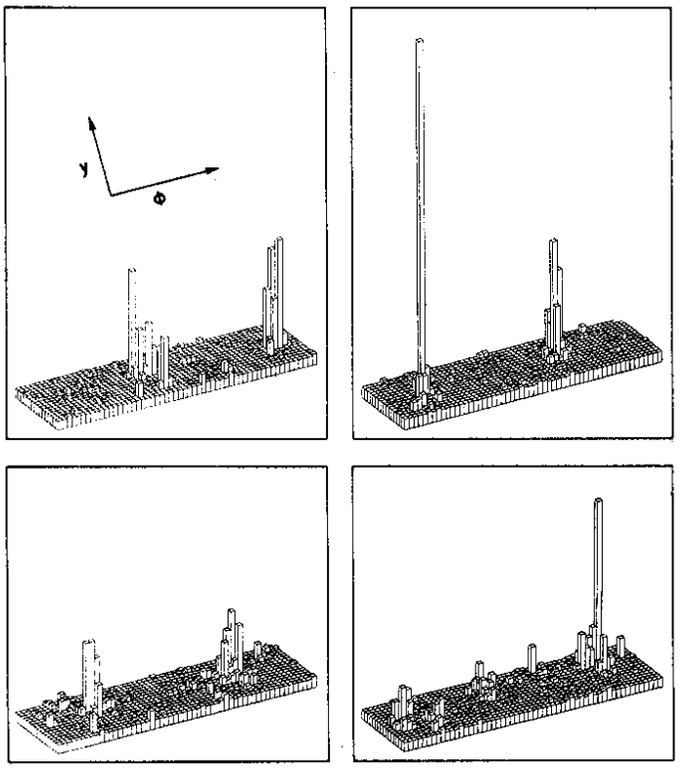

Fig. 10 Four events with E_T > 35 GeV measured by the AFS.

The result from the COR Collaboration presented in this section is described in more detail in Ref. 8 and the AFS result in Ref. 10. The rest of the talk will be devoted to results from the AFS only.

3. Jet fragmentation

It is clear from the data discussed in the previous section that in the high-E_T region the events are completely dominated by collimated particle showers. The natural thing to do next is to measure the fragmentation of these jets, and to compare them with the jets produced in e^+e^- annihilation events. The data used for this analysis are at $\sqrt{s}$ = 63 GeV, E_T > 33 GeV, and have a loose requirement on the event shape, C < 0.4.

The first thing we look for is the momentum distribution of the individual particles. At PETRA and PEP this is often measured as $d\sigma/dx_p$, where $x_p = p/p_{beam}$. In general, p is measured by the central drift chambers, i.e. for charged particles only. For pp collisions, $x_p = 2p/W'$, where W' is the centre-of-mass energy for the colliding partons. At the AFS, the individual charged-particle momenta p are measured by the central drift chamber. In order to estimate W' we use the information from the calorimeter. However, since not all the particles measured belong to the high-p_T jets, the invariant mass of *all* particles seen in the calorimeter will in general be an overestimate of W'. We are therefore forced to use a Monte Carlo[11] plus full detector simulation to enable us to estimate W'.

In the Monte Carlo we calculate the invariant mass of all particles with $p_T > 1$ GeV/c, which we estimate to be predominantly jet particles, obtaining a conversion factor between this invariant mass and W'. This is a correction $\sim$ 20%. In the data we now calculate the invariant mass of all particles with $p_T > 1$ GeV/c, and translate this to W' using the relation found by the Monte Carlo. We then plot the distribution of x_p measured for all particles in the central drift chamber. The distribution is normalized by the number of jets and compared with $(1/2\sigma_{had})\ d\sigma/dx_p$ measured by TASSO [12] and is shown in Fig. 11. The figure shows a very nice agreement between the jets in pp collisions and jets in e^+e^- annihilation events.

The next thing we study is the width of the jets.

In order to measure the width of the jets it is necessary to know the direction of the scattered constituents. Unlike e^+e^- jets, the constituent jets in hadron interactions are not generally collinear in the centre of mass of both beams; the colliding partons have different x-values and a contribution from initial transverse momentum k_T. The jet axis will be found by the calorimeter, and the individual particle momenta will be measured by the central drift chamber.

To find the jet axis we will use a cluster algorithm that was developed elsewhere [9]. The algorithm uses as a distance-measure the transverse momentum between the particles. The algorithm is provided with a cut-off parameter q_T^{cut} defining the largest allowed distance between two particles to be joined together. The procedure of the algorithm is as follows:

i) A pre-clustering is made by taking the highest momentum particle and joining to it all particles with a $q_T < 250$ MeV/c away from it. Of

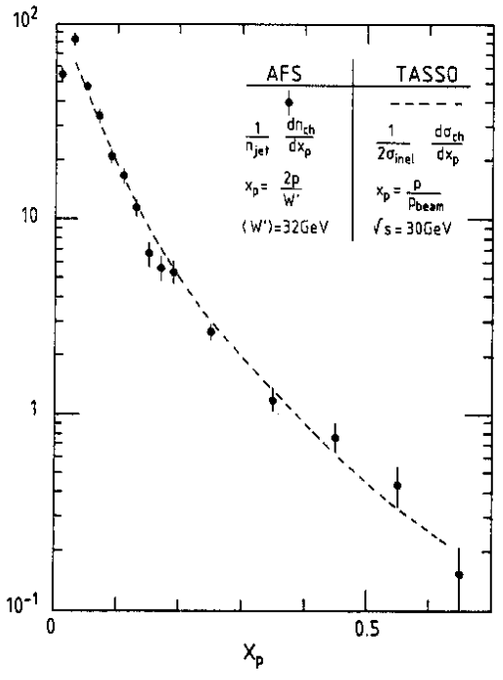

Fig. 11 The x_p-distribution measured by the AFS.

the remaining particles, the largest momentum particle is found, and all remaining particles with a q_T < 250 MeV/c are joined to it. This procedure is repeated until all clusters with q_T relative to another cluster of less than 250 MeV/c are merged.

ii) Using these pre-clusters, one finds the two closest clusters and, if their internal distance is less than q_T^{cut}, joins them. The procedure is repeated until one is left with a number of clusters, all with distances between any two clusters greater than q_T^{cut}. After each merging, the cluster algorithm checks whether all the particles are assigned to the closest cluster, and if not, it allows reassignment.

Figure 12 shows the result of using the cluster algorithm with different values on q_T^{cut}, on data, and on a high-p_T Monte Carlo[11] with detector simulation. From the result it can be seen that the fraction of events with more than two jets is strongly dependent on the cut-off value. In addition, it should be noted that for a given cut-off value the fraction of events with more than two jets is quite larger in the data than in the Monte Carlo. We will measure $\langle q_T \rangle$ in the data which satisfy the two-jet assumption when using the cluster algorithm on only particles with p_T > 1.0 GeV/c and with the cut-off parameter set to 4 GeV/c. In this case, the algorithm finds two jets in the majority of events. From the Monte Carlo, the mean angle between the initial parton direction and measured jet direction is found to be 4°. In Fig. 13 we plot $\langle q_T \rangle$ against z, where z is defined as the momentum component along the jet axis divided by $W_{\frac{1}{2}}$. Superimposed on the figure are predictions from the Monte Carlo. The solid line is obtained in the Monte Carlo with a jet width $\langle Q_T \rangle$ = 0.4, where Q_T is an internal parameter in the Monte Carlo setting the width of the jet fragmentation, and the dashed line is when the jet width is measured to $\langle Q_T \rangle$ = 0.65 GeV/c. Both lines include detector simulation. It is clear from the figure that the data favour $\langle Q_T \rangle$ = 0.65 GeV/c.

It should be noted that also in e^+e^-, if all events are analysed under a two-jet assumption, the $\langle q_T \rangle$ versus z observed is very similar to the one in Fig. 13. Our large value of $\langle Q_T \rangle$ may well reflect a broadening due to α_s^3 effects (e.g. gluon bremsstrahlung leading to three-jet events). It should be noted that in hadron-hadron scattering, inclusion of the three-jet process requires a calculation up to α_s^3 (cf. e^+e^- where the three-jet process is order α_s), and the Monte Carlo only goes to order α_s^2.

4. Charge distribution in the jets

Using global jet features such as the jet direction and W′, measured in the calorimeter, and the individual charged particle momenta measured by the central drift chamber, we can study the distribution of charges in the jets.

Figure 14 shows the ratio between positive and negative particles as a function of x_p, and a clear effect from the valence quark composition in the colliding protons is seen in the rising ratio. The next thing we

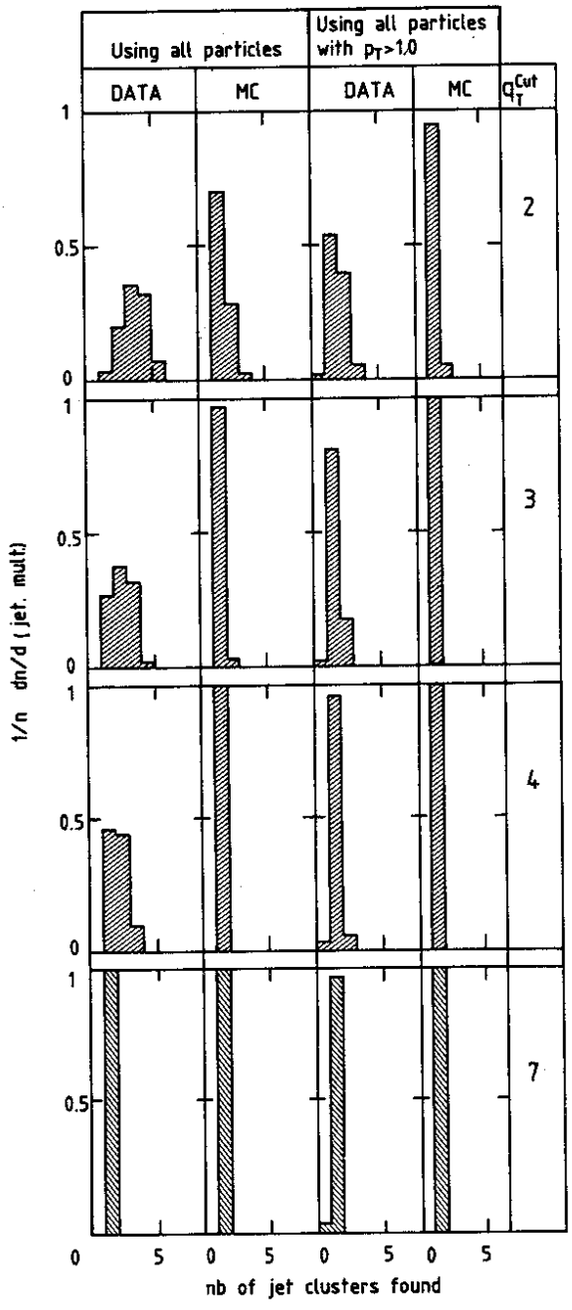

Fig. 12 Performance of the cluster algorithm[9] for different values of the cut-off parameter.

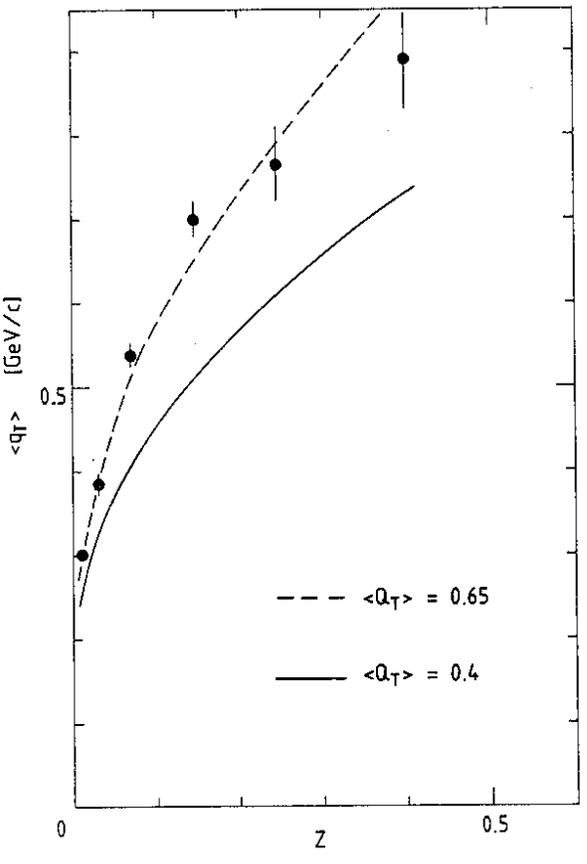

Fig. 13 Mean transverse momentum with respect to the jet axis as a function of z. The solid line shows the Monte Carlo for $\langle Q_T \rangle$ = 0.4 GeV/c and the dashed line for $\langle Q_T \rangle$ = = 0.65 GeV/c.

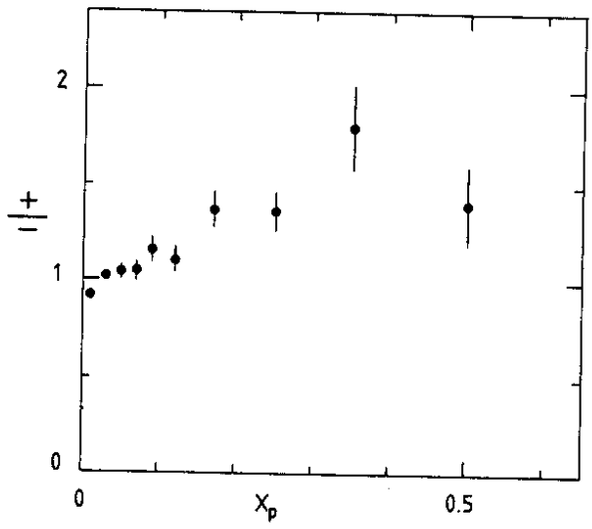

Fig. 14 The ratio of positive to negative particles as a function of x_p.

examine is the charge compensation within a jet and the charge correlation with the other jet[13]. We use the function

$$\Phi(y,y') = \left[(d^2\sigma/dydy')\text{ opposite charge} - (d^2\sigma/dydy')\text{same charge}\right]/(d\sigma/dy'),$$

where y and y′ are the rapidity along the jet axis of the individual particles. In Fig. 15 we show the variation of Φ with y′ fixed and various y. From the figure it is seen that the behaviour is rather different for a positive and a negative particle in a bin centred at y′. The difference in the long-range correlation can be seen by comparing Figs. 15e and 15h, where for negative y we get positive correlation with the negative trigger and anticorrelation for the positive trigger. The difference is easily understood as a consequence of having two valence u-quarks and only one valence d-quark. Thus, no matter what the "trigger" at y′ is, it is more probable to have a positive recoil jet. Figures 15c and 15g show that for a negative "trigger" at y′ near the central region the charge correlation is positive throughout the y range, whilst for a positive "trigger" it is positive only in the central region, and at high $|y|$ it becomes negative, again reflecting the higher probability of the leading charge to be positive. By comparing Fig. 15e with 15h and Fig. 15f with 15i, it is seen that the short-range charge compensation is stronger for a negative particle in y′ than for a positive one. Charge compensation has been studied in more detail for events with a single high-p_T particle trigger[14], and Fig. 16a shows the effect of a difference in short-range charge compensation when a negative particle is in y′ compared with a positive one. As can be seen in Fig. 16b, this effect seems to be dominated by associated non-pions.

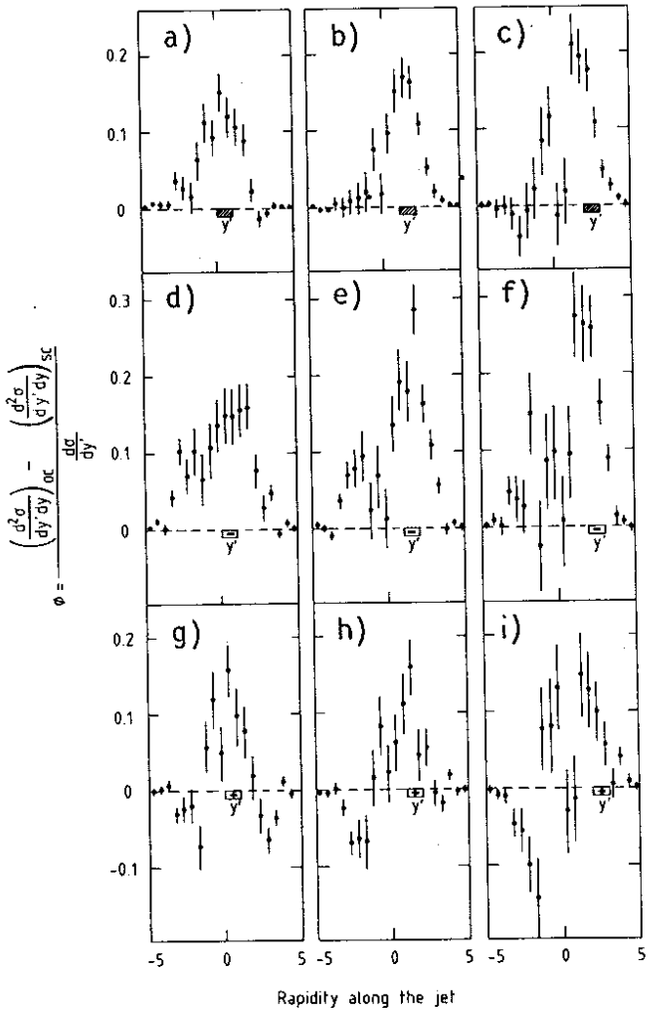

Fig. 15 Charge compensation as a function of rapidity along the jet axis: (a) to (c) all charges, (d) to (f) for negative "trigger", (g) to (i) for positive "trigger"; OC is opposite charge, SC is same charge.

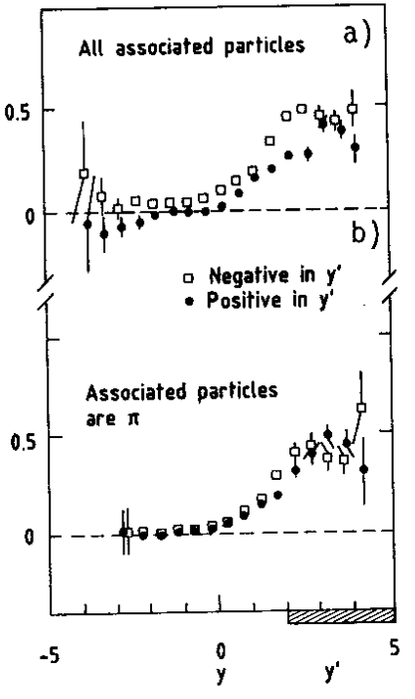

Fig. 16 Charge compensation as a function of rapidity along the jet axis for events with a high-p_T single-particle trigger: a) all associated particles; b) only pions as associated particles.

Conclusions

Calorimeter experiments at the ISR have considerably clarified the topic of high-p_T jets. The jet events are strikingly evident, which makes a direct comparison with e^+e^- events rather straightforward. Future measurements of charge compensation and flavours in these jets may give information about the relative contributions of qq, qg and gg scattering, and details in the fragmentation process.

Acknowledgements

I would like to acknowledge the careful work of my colleagues at the AFS, and to thank L. Camilleri and P.T. Cox of the COR Collaboration for helpful discussions. Finally, I would like to thank the organizers for an inspiring meeting at a beautiful place.

References and Footnotes

1) Proc. 21st Int. Conf. on High-Energy Physics, Paris, 1982 [J. Phys. 43 (1982)]:
   a) UA2 Collaboration, p. C3-571.
   b) AFS Collaboration, p. C3-122.

2) T. Åkesson et al., Phys. Lett. 118B (1982) 185.

3) T. Åkesson et al., Phys. Lett. 121B (1983) 133.

4) M. Banner et al., Phys. Lett. 118B (1982) 203.

5) G. Arnison et al., Phys. Lett. 121B (1983) 115.

6) CERN-Oxford-Rockefeller (COR) Collaboration:
   A.L.S. Angelis, G. Basini, H.-J. Besch, R.E. Breedon, L. Camilleri, T.J. Chapin, R.L. Cool, P.T. Cox, C. von Gagern, C. Grosso-Pilcher, D.S. Hanna, J.T. Linnemann, C.B. Newman, R.B. Nickerson, N. Phinney, S.H. Pordes, K. Powell, R.W. Rusack, A.M. Segar, M.J. Tannenbaum, and J.M. Yelton.

7) Brookhaven-Cambridge-CERN-Niels Bohr Institute-London (QMC)-Lund-Pennsylvania-Pittsburgh-Rutherford-Tel Aviv Collaboration:
   T. Åkesson, M.G. Albrow, S. Almehed, R. Batley, O. Benary, H. Bøggild, O. Botner, H. Breuker, H. Brody, V. Burkert, R. Carosi, A.A. Carter, J.R. Carter, P. Cecil, S.U. Chung, W.E. Cleland, D. Cockerill, S. Dagan, E. Dahl-Jensen, I. Dahl-Jensen, P. Dam, G. Damgaard, S. Eidelman, W.M. Evans, C.W. Fabjan, P. Frandsen, S. Frankel, W. Frati, M. Gibson, U. Goerlach, H. Gordon, A. Hallgren, K.H. Hansen, B. Heck, V. Hedberg, J. Hiddleston, H.J. Hilke, J. Hooper, G. Jarlskog, P. Jeffreys, T. Jensen, A. Kalinovsky, G. Kesseler, T. Killian, R. Kroeger, K. Kulka, J.v.d. Lans, J. Lindsay, D. Lissauer, B. Lörstad, T. Ludlam, A. Markou, N.A. McCubbin, U. Mjörnmark, R. Møller, W. Molzon, B.S. Nielsen, A. Nilsson, L.H. Olsen, Y. Oren, L. Rosselet, E. Rosso, A. Rudge,

R. Schindler, I. Stumer, M. Sullivan, G. Thorstenson, E. Vella, J. Williamson, W.J. Willis, M. Winik, W. Witzeling, C. Woody, and W.A. Zajc.

8) A.L.S. Angelis et al., Phys. Lett. 126B (1983) 132.

9) T. Sjöstrand, Comput. Phys. Common. 48 (1983) 229.

10) T. Åkesson et al., Phys. Lett. 128B (1983) 354.

11) H.U. Bengtsson, The Lund Monte Carlo for high-p_T physics, LU-TP 82-15 (1982).

12) R. Brandelik et al., Phys. Lett. 94B (1980) 437.

13) R. Brandelik et al., Phys. Lett. 100B (1981) 357.

14) T. Åkesson et al., Correlations with a charged particle of large transverse momentum. Paper given at the Int. Europhysics Conf. on High-Energy Physics, Brighton, UK, 20-27 July 1983.